Title: Immunodominant surface epitopes power immune evasion in the African trypanosome

Authors: Anastasia Gkeka[1,2†], Francisco Aresta-Branco[1,3†], Gianna Triller[1], Evi P. Vlachou[1], Mirjana Lilic[4], Paul Dominic B. Olinares[5], Kathryn Perez[6], Brian T. Chait[5], Renata Blatnik[7], Thomas Ruppert[7], C. Erec Stebbins[3*], F. Nina Papavasiliou[1*]

Affiliations:

[1]Division of Immune Diversity, German Cancer Research Center; Heidelberg, Germany.

[2]Faculty of Biosciences, University of Heidelberg, Heidelberg, Germany.

[3]Division of Structural Biology of Infection and Immunity, German Cancer Research Center; Heidelberg, Germany.

[4]The Rockefeller University, Laboratory of Structural Microbiology; New York, New York, USA.

[5]The Rockefeller University, Laboratory Of Mass Spectrometry And Gaseous Ion Chemistry; New York, New York, USA.

[6]Protein Expression and Purification Core Facility, EMBL Heidelberg; Heidelberg, Germany.

[7]Center for Molecular Biology of Heidelberg University, DKFZ-ZMBH Alliance; Heidelberg, Germany.

*Correspondence to: n.papavasiliou@dkfz-heidelberg.de, e.stebbins@dkfz-heidelberg.de

†These authors contributed equally.

Short title: Immunodominance can power immune evasion

Abstract

The African trypanosome survives the immune response of its mammalian host by antigenic variation of its major surface antigen (the Variable Surface Glycoprotein, or VSG). Here we describe the antibody repertoires elicited by different VSGs. We show that the repertoires are highly restricted, directed predominantly to epitopes on the surface of the VSGs. They are also highly discriminatory: minor alterations within these exposed epitopes confer antigenically-distinct properties to these VSGs and elicit different repertoires. We propose that the patterned and repetitive nature of the VSG coat focuses host immunity to a restricted set of immunodominant epitopes per VSG, eliciting a highly stereotyped response, minimizing cross reactivity between different VSGs and facilitating prolonged immune evasion through epitope variation.

One Sentence Summary: Hyper-focused antibody responses to variable antigenic coats allow pathogens to escape immune recognition.

Main Text:

The African trypanosome (*Trypanosoma brucei spp*) is a strictly extracellular parasite, infection with which elicits a robust antibody response against its Variant Surface Glycoprotein (VSG) coat (*1*, *2*). This response mediates parasite clearance and also enables immune escape of variants that have switched surface coat composition(*3*). The dynamic interplay between VSG-coat-switching by trypanosomes and the B cell response of the host that they evade is central to the maintenance of chronic infection (*4*).

Very little is known about the nature of the antibody response against the VSG coat. A small number of papers beginning in the 1990s revealed that acute infection with *T. brucei* leads to extraordinarily high levels of IgM in humans and in mice (*1*). The antibody response has often been characterized as polyclonal and many of those antibodies are autoreactive (*1*, *5*, *6*). However, these data are conceptualized in the context of a prolonged infection that itself is polyclonal in VSG-archetype. An understanding of the response to individual VSG variants in a controlled setting is therefore lacking, since the culmination of multiple separate responses to different VSGs would produce a "polyclonal" B cell output in the greater infection context. Importantly, immunization or exposure to specific VSG surface coats prevents later infection by cells expressing that same coat, indicating that coat-specific antibodies must be produced during infection (*3*, *7*).

To begin to explore the parameters of the antibody response to *T. brucei*, we examined the antibody repertoires elicited by two specific VSGs. These were chosen to broadly represent the two primary VSG "classes": VSG2 (a class-A VSG) and VSG3 (a class-B VSG) (*8*). To do this we infected animals with each specific VSG-expressing parasite, and either "cleared" the parasite with the anti-protozoan compound diminazene four days after infection (as often infection is

63 rapidly lethal) (*9*) or allowed the animals to clear the parasite naturally (whenever feasible) after
64 the first peak of parasitemia (at which point the parasites that have switched VSG coats remain
65 and seed the next peak of parasitemia). Initial analyses of infected C57BL/6 mice showed a robust
66 expansion of plasma cells (Fig. 1A, Fig. S1A). This expansion was common to all infections
67 regardless of whether parasites were cleared by the animals (usually by day 6 or day 7 post
68 infection) or whether they were pharmacologically cleared earlier with diminazene (days 4 and 5),
69 allowing for the maturation of the antibody response until collection (which was uniformly at day
70 8 post infection – Fig. 1B). This is also consistent with known parameters of disease progression
71 (*3*, *10*, *11*).

72 Typically, the characterization of an antigen-specific antibody repertoire benefits from the
73 "baiting" of antigen specific B cells using the antigen itself conjugated to a fluorophore (PE or
74 APC) (*12*, *13*). However, plasma cells are notoriously hard to bait as they downregulate surface
75 expression of Ig and rather secrete the vast majority of the antibody they produce, so that very little
76 antibody remains surface-bound and accessible. We therefore proceeded to sort all plasma cells
77 according to surface marker expression (CD138+/CD19^{lo}) (*14*) into 384-well plates. The antibody
78 repertoire of plasma cells was then assembled after two rounds of single cell PCR and paired heavy
79 (IgH) and light (Igκ/λ) gene sequence analysis (*12*).

80 We first focused on the repertoire elicited by VSG2-coated parasites. Surprisingly for a non-
81 baited repertoire, plasma cells elicited from mice infected with VSG2 were dominated by cells
82 carrying only four VH+VL chain pairings (VH10.1 or VH10.3 with VL19-20 or VL19-14, Fig.
83 1C). These combinations, which are absent in naïve mice (Fig. S1B), formed the plurality of the
84 repertoire when mice were pharmacologically treated to remove trypanosomes four days after
85 infection, but they became increasingly prevalent in repertoires of animals that cleared

86 trypanosomes naturally a day before collection, and even more dominant in repertoires of animals
87 that cleared the infection the day we collected plasma cells (Fig. 1C). This suggests a rapid and
88 robust response to the parasite, stereotyped between mice, that becomes increasingly diversified
89 as more antigens become available after parasite lysis.

90 We reasoned that the repertoire we collected closest to natural clearance would contain the B
91 cells likely expressing the most potent anti-coat-specific antibodies and proceeded to analyze it
92 further. While dominated by cells expressing two distinct immunoglobulin (Ig) heavy and Ig light
93 chain gene pairs, the B cells elicited by VSG2-coated *T. brucei* were not monoclonal: each VH10
94 heavy and 19-20 or 19-14 light chain V region was joined to a variety of DJ or J gene segments
95 representing a wide swath of CDR3 (Fig. 1D and Supplemental file 1). This lack of clonal
96 expansion is also evident from the Shannon entropy index on a sequence level (Fig. 1C, bottom of
97 each circos plot).

98 We therefore picked a small number of heavy and light chain pairs from the overrepresented
99 V gene segments identified and proceeded to express them recombinantly as soluble antibodies in
100 293T cells. Indeed, 7 out of 11 of these antibodies are capable of binding live, VSG2-coated *T.*
101 *brucei*, but not parasite cells coated with a different VSG protein (Fig. 1D, Fig. 2F). Antibodies
102 that did not use these V segments were not able to bind VSG2-coated parasites (Fig. S2). We
103 conclude that the VSG2-elicited plasma cell repertoire represents an oligoclonal expansion
104 primarily of four variable region defined pairs, which are mostly unmutated (Fig. 1D and
105 Supplemental file 1). The V gene signature that defines this repertoire is stereotyped between mice
106 (Fig. 1C), suggesting both that the VSG2-specific paratope is likely located within highly specific
107 variable regions of the antibody protein, and that these antibodies are likely generated against a
108 common immunodominant epitope.

109 Epitope identification is often achieved by structural analyses of repertoire-defined antibodies
110 together with the antigen that elicited them (*15*). We therefore sought to crystallize VSG2
111 (specifically, the larger, surface-exposed N-terminal domain of the VSG, or "NTD") together with
112 VSG2-specific Fab-fragments. All crystals obtained were of VSG2 alone, however (Fig. S3A,
113 Table S2), likely because most antibodies elicited by *T. brucei* infection are of the IgM isotype
114 (Fig. S4) (*1*) and are likely of low affinity (but high avidity); therefore, they do not bind with high-
115 affinity when produced recombinantly as an IgG (or Fab) fragment (as current methods for the
116 recombinant production of pentameric IgM are poorly optimized). Serendipitously, the crystals
117 did allow us to re-solve the structure of VSG2 to much higher resolution compared to previous
118 work (*16*, *17*), with unexpected findings. The protein structure of VSG2 from these new crystals
119 is nearly identical to that from the 1990 crystal form, with a root-mean-square deviation of 0.87Å
120 over 1420 atoms of a monomer in the dimer (Fig. 2A, Fig. S5). However, in later stages of model
121 refinement, unusually large electron density around solvent molecules was modeled effectively
122 with calcium (Fig. 2, B and C), an ion not present in older structures likely due to the use of
123 chelating agents in the purification from animal blood (*18*, *19*). Calcium is octahedrally
124 coordinated in VSG2 through a network of oxygen bonds: four from three consecutive amino acid
125 side-chains at the end of a β-strand (bidentate-D208, N209, and D210, henceforth the "DND
126 motif"), the carbonyl-oxygen from G155 in an opposing loop, and three water molecules in the
127 solvent shell above the protein (each water coordinated by other side-chain and main-chain
128 contacts from the protein, Fig. 2C).

129 There is little change in the fold or amino acid side-chain positioning between the calcium
130 bound and free structures of VSG2 (Fig. 2, A-C), indicating that the pocket does not undergo any
131 significant conformational changes upon calcium binding. The presence of calcium was verified

132 both by mass spectrometry as well as isothermal titration calorimetry (Fig. S6). The calcium
133 binding pocket in VSG2 appears to be unique, not closely resembling any published structures in
134 the PDB (e.g., DALI homology search) (*20*). The pocket occurs near the "top" of the NTD of
135 VSG2, slightly sheltered from the uppermost surface (Fig. 2A). A triple mutation of the DND
136 motif to alanine ($VSG2_{AAA}$) abrogates calcium binding (Fig. S3B and S5) without any significant
137 conformational changes (Figure 1, A and C), although electrostatic surfaces generated from the
138 three structures show an expected change to a more neutral charge distribution in the pocket region
139 of the mutant (Fig. 2D).

140 Unexpectedly, despite the high similarity between the wild type and mutant structures,
141 antisera elicited by infection with $VSG2_{WT}$ coated trypanosomes, do not bind trypanosomes
142 expressing the minor variant represented by the $VSG2_{AAA}$ mutant (Fig. 2E). Furthermore, our
143 recombinantly expressed antibodies specific to the $VSG2_{WT}$ coat were unable to bind the $VSG2_{AAA}$
144 mutant coat (Fig. 2F, Fig. S2), despite the fact that these mutations did not cause conformational
145 changes in VSG2 (Fig. 2, A and C, Fig. S6). This suggests that the VSG2 epitope recognized by
146 both antisera and monoclonal antibodies is located within the region defined by the DND motif
147 and conversely, that antibodies to VSG2-coated trypanosomes are capable of a high degree of
148 epitope discrimination.

149 To assess whether this combination of epitope immunodominance and antibody
150 discrimination characterizes the epitope space of other VSGs, we analyzed antibody repertoires
151 from plasma cells collected from animals infected with VSG3-coated trypanosomes. VSG3 is a
152 member of a different VSG class with significant structural and post-translational modifications
153 distinguishing it from VSG2 (class A vs class B VSGs, respectively) (*8*). Previously, we had solved
154 the crystal structure of the VSG3 NTD, leading to the unexpected identification of an *O*-linked

155 glycosylation of a serine residue (S317, heterogeneously modified with 0-3 hexose residues)
156 located in the center of the top surface of the protein (*21*). Mutation of that serine to an alanine
157 residue ablated glycosylation, reduced parasite virulence, and enhanced the effectiveness of the
158 host immune response (*21*). At the time we hypothesized that this was due to the tendency of *O*-
159 linked sugars to adopt multiple conformational states (*22*), thus further diversifying the epitope
160 space of the VSG3 coat. Therefore, to assess whether VSG3 coated trypanosomes lacking this
161 post-translational modification could also elicit a stereotyped immune response toward an
162 immunodominant epitope (such as we have seen for VSG2-coated parasites), we first infected mice
163 with S317A mutant parasites ($VSG3_{S317A}$), and analyzed the resulting plasma cell antibody
164 responses either after natural clearance or after treatment with diminazene. As was the case for
165 VSG2 coated parasites, $VSG3_{S317A}$ coated parasites were also capable of reproducibly eliciting a
166 restricted B cell repertoire in multiple distinct infections (Fig. 3A). However, this repertoire was
167 now defined by a major light chain V gene (VL_gn33) pairing with a larger number of heavy
168 chains (Fig. 3A). Again, recombinant expression of a number of these heavy and light chain pairs
169 as secreted IgG1s in 293T cells show that many of the antibodies elicited by $VSG3_{S317A}$ coats are
170 capable of binding their cognate parasites (Fig. 3, C and D, Fig. S7). Although the common light
171 chain variable gene (gn33) is clearly important for binding, the proper heavy chain is also
172 necessary, since pairing of the gn33 light chain with a different VH can result in a loss of binding
173 (Fig. S8). Whether the common light chain plays a role in increasing antibody binding to the
174 repetitive coat remains to be investigated.

175 We also analyzed the resulting plasma cell response after infection with $VSG3_{WT}$ followed by
176 treatment with diminazene (the high virulence of the strain is incompatible with natural clearance).
177 We found that the light-chain restriction seen with $VSG3_{S317A}$ elicited repertoires is now entirely

178 abolished, strongly suggesting that the addition of up to 3 *O*-linked hexoses per VSG3 molecule
179 functions to diversify the presumed immunodominant epitope presented by the $VSG3_{S317A}$ coated
180 parasite (Fig. 3B). Furthermore, the addition of sugars entirely prevented the major VL (gn33)
181 carrying antibody pairs from binding $VSG3_{WT}$ coated parasites (Fig. 3, C and D), suggesting that
182 antibodies elicited to the parasite coat are focused near-exclusively on the epitope that contains the
183 *O*-linked hexoses. Conversely, of the four antibodies we reconstituted and tested that were elicited
184 by the wildtype ($VSG3_{WT}$) infection, three were able to bind the sugarless coat, and one was
185 selective to the sugar on S317 (capable only of binding the wildtype) (Fig. 3, C and D).

186 A comparison of mutant and wild type structures verified that the protein surface between
187 the two VSG3 variants was identical (Fig. 4A) but yielded a surprise in the form of an additional
188 sugar in a neighboring serine (S319). We confirmed this in the $VSG3_{WT}$ structure by re-solving it
189 (Fig. 4, A and B, Fig. S9A, Fig. S10, Table S3). S319 is part of the surface-exposed loop harboring
190 S317, and in a previous study (*21*), both by crystallography and mass spectrometry, glycosylation
191 of S319 was not clearly present (likely due to intrinsic lability of the moiety). However, here we
192 were able to observe strong density for the sugar on S319 in the $VSG3_{WT}$ and $VSG3_{S317A}$ mutant
193 crystal structures, as well as to confirm the presence of hexose groups on S317 and S319 by mass
194 spectrometry (Fig. S11). Subsequent determination of the crystal structures of the S319A mutant
195 as well as the double mutant (combining S317A and S319A, or "SSAA") did not reveal any
196 significant structural differences when compared to $VSG3_{WT}$ or $VSG3_{S317A}$ (Fig. 4, A and B, Fig.
197 S9, B-D, Fig. S10).

198 Following the experimental protocol that we had used to assess the quality of the repertoires
199 elicited by $VSG3_{WT}$ and $VSG3_{S317A}$, we also generated plasma cell antibody repertoires elicited by
200 $VSG3_{S319A}$ and $VSG3_{SSAA}$, (Fig. 4C) and tested those for their ability to bind either their cognate

201 parasites or to cross-react with the wild type and other mutants. We found that $VSG3_{SSAA}$ parasites
202 elicited repertoires very similar to those elicited by the $VSG3_{S317A}$ mutant alone (e.g. dominant
203 presence of the gn33 light chain V gene and 30-60.6.70 or J558.26.116 heavy chain gene), whereas
204 $VSG3_{S319A}$ single mutants elicited broader repertoires that were very similar to those elicited by
205 $VSG3_{WT}$ (no gn33 dominance for example) (Fig. 4C). In turn, this suggests that the $VSG3_{WT}$
206 repertoire is strongly influenced by the one-to-three hexoses linked to S317 (*21*) but negligibly by
207 the glycans linked to S319; similarly, that the S317A determined repertoire is indifferent to the
208 presence of the sugar on S319, as the repertoire does not change in the double mutant.

209 These results underscore the immunodominance of the relevant epitopes and the exquisite
210 discrimination of the resulting antibodies. Specifically, they suggest that the immunodominant
211 epitope that characterizes the $VSG3_{WT}$ coat is limited to the immediate amino-acids surrounding
212 the S317-*O*-glucose (including that sugar but excluding its companion on S319). Consequently,
213 when we tested recombinant antibodies that were elicited after infection with each of these variants
214 for the ability to cross-react with each of the other variants, we identified four classes of binders:

215 (a) Antibodies that could bind all four variants (like ab239 or ab222, Fig. 4, D and E); these
216 were elicited by both $VSG3_{WT}$ and $VSG3_{SSAA}$ suggesting that they bind a common peptide
217 epitope at a distance from the epitope defining sugar.

218 (b) Antibodies that bound only the epitope-defining sugar-containing variants $VSG3_{WT}$ and
219 $VSG3_{S319A}$ (like ab250, Fig. 4, D and E) but not the other two variants; suggesting that they bind
220 the sugar containing epitope but not the same epitope without the carbohydrate (and are therefore
221 potentially sugar-selective);

222 (c) Antibodies that bound only the variants that lacked the epitope-defining sugar at S317
223 (VSG3$_{S317A}$ and VSG3$_{SSAA}$, like ab021); suggesting that they bind the same peptide epitope
224 defined by the sugar but are inhibited by the presence of the sugar in the other two variants.
225 (d) Finally, antibodies that only bound the VSG3$_{S317A}$ variant (e.g. ab234), potentially
226 suggestive of an additional minor epitope partly defined by the S319 sugar.

227 Overall, by examining two distinct VSGs and variants thereof, we demonstrate that the
228 antibody response that mediates clearance to a given *T. brucei* coat can be hyperfocused to a
229 restricted set of immunodominant epitopes that are surface exposed. Consequently, the immune
230 response elicited by each *T. brucei* variant coat has the potential to be highly restricted and likely
231 mediated by paratopes within the germline V regions of antibody genes. How *T. brucei* achieves
232 this "immunofocusing" is likely related to the highly dense, repetitive and patterned nature of its
233 surface coat. We hypothesize that this extreme focusing allows the parasite to use short-tract gene
234 conversion or even point mutations (collectively referred to as mosaic formation (*3*, *23*)) to expand
235 its antigenicity well beyond what is encoded in its considerable genomic archive. By ensuring that
236 cross reactivity between coat-defined epitopes will be exceedingly rare, even within similar
237 variants, immunofocusing helps the parasite perpetually evade the immune response.

238

239

240

241

242

243

References and Notes:

1. J. Verdi, R. Zipkin, E. Hillman, R. A. Gertsch, S. J. Pangburn, R. Thomson, N. Papavasiliou, J. Sternberg, J. Raper, Inducible Germline IgMs Bridge Trypanosome Lytic Factor Assembly and Parasite Recognition. *Cell Host and Microbe*. **28**, 79-88.e4 (2020).
2. B. Stijlemans, M. Radwanska, C. de Trez, S. Magez, African trypanosomes undermine humoral responses and vaccine development: Link with inflammatory responses? *Frontiers in Immunology*. **8** (2017), doi:10.3389/fimmu.2017.00582.
3. M. R. Mugnier, G. A. M. Cross, F. N. Papavasiliou, The in vivo dynamics of antigenic variation in *Trypanosoma brucei*. *Science*. **347**, 1470–1473 (2015).
4. S. Silva-Barrios, T. Charpentier, S. Stäger, The Deadly Dance of B Cells with Trypanosomatids. *Trends in Parasitology*. **34**, 155–171 (2018).
5. N. Müller, J. M. Mansfield, T. Seebeck, Trypanosome Variant Surface Glycoproteins Are Recognized by Self-Reactive Antibodies in Uninfected Hosts. *Infection and Immunity*. **64**, 4593–4597 (1996).
6. P. Diffley, Trypanosomal surface coat variant antigen causes polyclonal lymphocyte activation. *J Immunol.* **131**, 1983–1986 (1983).
7. G. H. Campbell, K. M. Esser, F. I. Weinbaum, *Trypanosoma rhodesiense* Infection in B-Cell-Deficient Mice. *Infection and Immunity*. **18**, 434–438 (1977).
8. M. Carrington, N. Miller, M. Blum, I. Roditi, D. Wiley, M. Turner, Variant Specific Glycoprotein of *Trypanosoma brucei* Consists of Two Domains each Having an Independently Conserved Pattern of Cysteine Residues. *J. Mol. Biol*. **221**, 823–835 (1991).

268 9. J. Pinger, S. Chowdhury, F. N. Papavasiliou, Variant surface glycoprotein density
269 defines an immune evasion threshold for African trypanosomes undergoing antigenic
270 variation. *Nature Communications*. **8** (2017), doi:10.1038/s41467-017-00959-w.
271 10. S. J. Black, C. N. Sendashonga, C. O'brien, N. K. Borowy, M. Naessens, P. Webster,
272 M. Murray, "Regulation of Parasitaemia in Mice Infected with *Trypanosoma brucei*"
273 in *The Biology of Trypanosomes. Current Topics in Microbiology and Immunology*
274 (Springer), vol. 117, pp. 93–118 (1985).
275 11. S. Jayaraman, C. Harris, E. Paxton, A. M. Donachie, H. Vaikkinen, R. McCulloch,
276 J. P. J. Hall, J. Kenny, L. Lenzi, C. Hertz-Fowler, C. Cobbold, R. Reeve, T. Michoel,
277 L. J. Morrison, Application of long read sequencing to determine expressed antigen
278 diversity in *Trypanosoma brucei* infections. *PLoS Neglected Tropical Diseases*. **13**
279 (2019), doi:10.1371/journal.pntd.0007262.
280 12. T. Tiller, E. Meffre, S. Yurasov, M. Tsuiji, M. C. Nussenzweig, H. Wardemann,
281 Efficient generation of monoclonal antibodies from single human B cells by single
282 cell RT-PCR and expression vector cloning. *Journal of Immunological Methods*.
283 **329**, 112–124 (2008).
284 13. J. F. Scheid, H. Mouquet, N. Feldhahn, B. D. Walker, F. Pereyra, E. Cutrell, M. S.
285 Seaman, J. R. Mascola, R. T. Wyatt, H. Wardemann, M. C. Nussenzweig, A method
286 for identification of HIV gp140 binding memory B cells in human blood. *Journal of*
287 *Immunological Methods*. **343**, 65–67 (2009).
288 14. K. Pracht, J. Meinzinger, P. Daum, S. R. Schulz, D. Reimer, M. Hauke, E. Roth, D.
289 Mielenz, C. Berek, J. Côrte-Real, H. M. Jäck, W. Schuh, A new staining protocol for

290 detection of murine antibody-secreting plasma cell subsets by flow cytometry.
291 *European Journal of Immunology*. **47**, 1389–1392 (2017).
292 15. G. Triller, S. W. Scally, G. Costa, M. Pissarev, C. Kreschel, A. Bosch, E. Marois, B.
293 K. Sack, R. Murugan, A. M. Salman, C. J. Janse, S. M. Khan, S. H. I. Kappe, A. A.
294 Adegnika, B. Mordmüller, E. A. Levashina, J. P. Julien, H. Wardemann, Natural
295 Parasite Exposure Induces Protective Human Anti-Malarial Antibodies. *Immunity*.
296 **47**, 1197-1209.e10 (2017).
297 16. D. Freymann, J. Down, M. Carrington, I. Roditi, M. Turner, D. Wiley, 2.9 A
298 Resolution Structure of the N-terminal Domain of a Variant Surface Glycoprotein
299 from *Trypanosoma brucei*. *J. Mol. Biol*. **216**, 141–160 (1990).
300 17. P. Metcalf, M. Blum, D. Freymann, M. Turner, D. C. Wiley, Two Variant Surface
301 Glycoproteins of *Trypanosoma brucei* of different sequence classes have similar 6A
302 resolution X-ray structures. *Nature*. **325**, 84–86 (1987).
303 18. G. A. M. Cross, Identification, purification and properties of clone-specific
304 glycoprotein antigens constituting the surface coat of *Trypanosoma brucei*.
305 *Parasitology*. **71**, 393–417 (1975).
306 19. G. A. M. Cross, Release and Purification of *Trypanosoma brucei* Variant Surface
307 Glycoprotein. *Journal of Cellular Biochemistry*. **24**, 79–90 (1984).
308 20. L. Holm, DALI and the persistence of protein shape. *Protein Science*. **29**, 128–140
309 (2020).
310 21. J. Pinger, D. Nešić, L. Ali, F. Aresta-Branco, M. Lilic, S. Chowdhury, H. S. Kim, J.
311 Verdi, J. Raper, M. A. J. Ferguson, F. N. Papavasiliou, C. E. Stebbins, African

312 trypanosomes evade immune clearance by O-glycosylation of the VSG surface coat.
313 *Nature Microbiology*. **3**, 932–938 (2018).
314 22. E. Lisowska, The role of glycosylation in protein antigenic properties. *CMLS, Cell.*
315 *Mol. Life Sci*. **59**, 445–455 (2002).
316 23. J. P. J. Hall, H. Wang, J. David Barry, Mosaic VSGs and the Scale of *Trypanosoma*
317 *brucei* Antigenic Variation. *PLoS Pathogens*. **9** (2013),
318 doi:10.1371/journal.ppat.1003502.
319 24. S. Alsford, T. Kawahara, L. Glover, D. Horn, Tagging a *T. brucei* RRNA locus
320 improves stable transfection efficiency and circumvents inducible expression
321 position effects. *Molecular and Biochemical Parasitology*. **144**, 142–148 (2005).
322 25. H. Hirumi, K. Hirumi, Continuous Cultivation of *Trypanosoma brucei* Blood
323 Stream Forms in a Medium Containing a Low Concentration of Serum Protein
324 without Feeder Cell Layers. *The Journal of Parasitology*. **75**, 985–989 (1989).
325 26. G. Burkard, C. M. Fragoso, I. Roditi, Highly efficient stable transformation of
326 bloodstream forms of *Trypanosoma brucei*. *Molecular and Biochemical*
327 *Parasitology*. **153**, 220–223 (2007).
328 27. J. Ye, N. Ma, T. L. Madden, J. M. Ostell, IgBLAST: an immunoglobulin variable
329 domain sequence analysis tool. *Nucleic acids research*. **41**, W34–W40 (2013).
330 28. P. D. Adams, P. v. Afonine, G. Bunkóczi, V. B. Chen, I. W. Davis, N. Echols, J. J.
331 Headd, L. W. Hung, G. J. Kapral, R. W. Grosse-Kunstleve, A. J. McCoy, N. W.
332 Moriarty, R. Oeffner, R. J. Read, D. C. Richardson, J. S. Richardson, T. C.
333 Terwilliger, P. H. Zwart, PHENIX: A comprehensive Python-based system for

334 macromolecular structure solution. *Acta Crystallographica Section D: Biological*
335 *Crystallography*. **66**, 213–221 (2010).
336 29. P. D. B. Olinares, B. T. Chait, "Native Mass Spectrometry Analysis of Affinity-
337 Captured Endogenous Yeast RNA Exosome Complexes" in *The Eukaryotic RNA*
338 *Exosome, Methods and Protocols Methods in Molecular Biology* (Clifton, N.J), vol.
339 2062, pp. 357–382 (2020).
340 30. D. J. Reid, J. M. Diesing, M. A. Miller, S. M. Perry, J. A. Wales, W. R. Montfort,
341 M. T. Marty, MetaUniDec: High-Throughput Deconvolution of Native Mass
342 Spectra. *Journal of the American Society for Mass Spectrometry*. **30**, 118–127
343 (2019).
344 31. M. T. Marty, A. J. Baldwin, E. G. Marklund, G. K. A. Hochberg, J. L. P. Benesch,
345 C. v. Robinson, Bayesian deconvolution of mass and ion mobility spectra: From
346 binary interactions to polydisperse ensembles. *Analytical Chemistry*. **87**, 4370–4376
347 (2015).
348 32. S. E. Zamze, D. A. Ashford, E. W. Wooten, T. W. Rademacher, R. A. Dwek,
349 Structural characterization of the asparagine-linked oligosaccharides from
350 *Trypanosoma brucei* Type II and Type III variant surface glycoproteins. *Journal of*
351 *Biological Chemistry*. **266**, 20244–20261 (1991).
352 33. A. Mehlert, J. M. Richardson, M. A. J. Ferguson, Structure of the
353 Glycosylphosphatidylinositol Membrane Anchor Glycan of a Class-2 Variant
354 Surface Glycoprotein from *Trypanosoma brucei*. *Journal of Molecular Biology*.
355 **277**, 379–392 (1998).

356 34. S. Manthri, M. L. S. Güther, L. Izquierdo, A. Acosta-serrano, M. A. J. Ferguson,
357 Deletion of the TbALG3 gene demonstrates site-specific N-glycosylation and N-
358 glycan processing in *Trypanosoma brucei*. *Glycobiology*. **18**, 367–383 (2008).
359 35. C. Fecher-Trost, U. Wissenbach, A. Beck, P. Schalkowsky, C. Stoerger, J. Doerr, A.
360 Dembek, M. Simon-Thomas, A. Weber, P. Wollenberg, T. Ruppert, R. Middendorff,
361 H. H. Maurer, V. Flockerzi, The in vivo TRPV6 protein starts at a non-AUG triplet,
362 decoded as methionine, upstream of canonical initiation at AUG. *Journal of*
363 *Biological Chemistry*. **288**, 16629–16644 (2013).
364
365

Acknowledgments: We acknowledge synchrotron time at the Paul Scherrer Institut, Villigen, Switzerland (SLS, beamline X06DA, Vincent Olieric and colleagues), the Diamond Light Source (DLS, beamline i03, Neil Paterson and colleagues) and the Advanced Photon Source, Argonne National Laboratory (APS, beamline 24-ID-C, Jonathan P. Schuermann and colleagues). We thank Johan P. Zeelen for assistance with the synchrotron data acquisition and advice in structural determination. We thank Hedda Wardemann for assistance with B cell repertoire analyses and fruitful discussions especially during manuscript revision. We are grateful to Joey Verdi for beneficial comments and discussion during manuscript revision. **Funding:** Work in the F.N.P and C.E.S labs is funded by the Helmholtz Foundation. P.D.B.O and B.T.C are funded by National Institutes of Health P41 GM109824 and P41 GM103314 to B.T.C. R.B and T.R. are supported by the German Research Foundation to T. R. (Ru 747/1-1) within in the framework of FOR 2509.
Author contributions: Conceptualization, Resources and Funding acquisition: F.N.P., C.E.S., Investigation: A.G., F.A.B., G.T., E.P.V., M.L., C.E.S., Mass Spectrometry (MS) analysis: P.D.B.O., B.T.C., R.B., T.R., ITC analysis: K.P., Formal Analysis: A.G., F.A.B., C.E.S., P.D.B.O.(MS), B.T.C.(MS), K.P.(ITC), R.B.(MS), T.R.(MS), Visualization: A.G., F.A.B., C.E.S., P.D.B.O.(MS), B.T.C.(MS), K.P.(ITC), R.B.(MS), T.R.(MS) Writing – Initial manuscript: F.N.P., C.E.S., Writing – Revised manuscript: F.N.P., C.E.S., A.G., F.A.B., G.T. **Competing interests:** Authors declare no competing interests. **Data and materials availability:** PDB IDs: 7P56 ($VSG2_{WT}$), 7P57 ($VSG2_{AAA}$), 7P59 ($VSG3_{WT}$), 7P5A ($VSG3_{S317A}$), 7P5B ($VSG3_{S319A}$), 7P5D ($VSG3_{SSAA}$); Mass spectrometry data are available via ProteomeXchange with identifier PXD027384. All other data is available in the main text or the supplementary materials.

Supplementary Materials:

Materials and Methods

Figures S1-S12

Tables S1-S4

References (*24-35*)

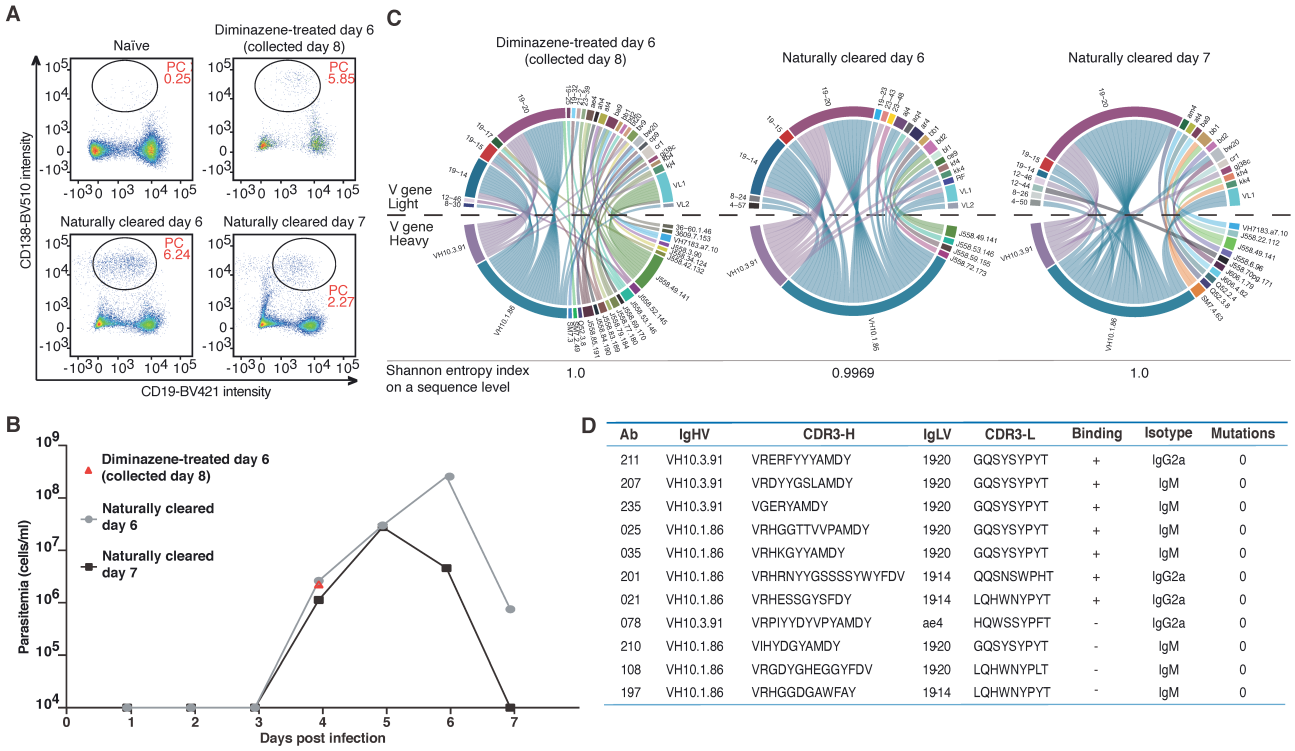

Ab	IgHV	CDR3-H	IgLV	CDR3-L	Binding	Isotype	Mutations
211	VH10.3.91	VRERFYYYAMDY	1920	GQSYSYPYT	+	IgG2a	0
207	VH10.3.91	VRDYYGSLAMDY	1920	GQSYSYPYT	+	IgM	0
235	VH10.3.91	VGERYAMDY	1920	GQSYSYPYT	+	IgM	0
025	VH10.1.86	VRHGGTTVVPAMDY	1920	GQSYSYPYT	+	IgM	0
035	VH10.1.86	VRHKGYYAMDY	1920	GQSYSYPYT	+	IgM	0
201	VH10.1.86	VRHRNYYGSSSSYWYFDV	1914	QQSNSWPHT	+	IgG2a	0
021	VH10.1.86	VRHESSGYSFDY	1914	LQHWNYPYT	+	IgG2a	0
078	VH10.3.91	VRPIYYDYVPYAMDY	ae4	HQWSSYPFT	-	IgG2a	0
210	VH10.1.86	VIHYDGYAMDY	1920	GQSYSYPYT	-	IgM	0
108	VH10.1.86	VRGDYGHEGGYFDV	1920	LQHWNYPLT	-	IgM	0
197	VH10.1.86	VRHGGDGAWFAY	1914	LQHWNYPYT	-	IgM	0

Fig.1: VSG2$_{WT}$ parasites elicit a highly restricted antibody repertoire, defined by a small number of heavy and light chain pairs. (A) Percentage of CD138+ plasma cells (PC) within the live lymphocyte population in a non-infected naïve mouse and in infected mice that were treated with diminazene or that naturally cleared the first peak of parasitemia. Plasma cells from this gate were sorted for antibody repertoire analysis. Representative gatings to determine live lymphocytes are shown in Supplementary Figure 1A. **(B)** Parasitemia infection curves from the 2 mice that naturally cleared the first peak of parasitemia (panel A) at day 6 (black) and day 7 (grey). Both mice were sacrificed at day 7 post-infection. A representative value of parasitemia at day 4 for mice treated with diminazene is indicated in red. **(C)** Circos plots generated for the VSG2$_{WT}$ V gene signatures of two independent mice whose infections were treated with diminazene (left - n=89 pairs) and of two additional mice that naturally cleared the first peak of parasitemia at days 6 (center - n=53 pairs) and 7 (right - n=50 pairs) post infection. Different colors depict each heavy

407 chain variable gene (bottom half of the plot), and each light chain variable gene (top half of the
408 plot). The heavy and light chain variable gene pairings that form the antibodies are illustrated as
409 connector lines starting from the heavy chain genes, providing also information about the
410 frequency of the pairings. Genes from both chains that appeared only once and resulted in single
411 heavy-light pairings, were considered background and were removed from the plot. Shannon
412 entropy shows clonal diversity on a sequence level with a value of 1.0 representing 100% clonal
413 diversity (no clones), while a value of 0.0 corresponding to 0% clonal diversity (only clones). **(D)**
414 Table with representative $VSG2_{WT}$ antibodies elicited in the context of diminazene-treated
415 infections, which are mostly composed of V*H*10 heavy chains paired with 19-14 and 19-20 Vκ
416 light chains. The CDR3 from each antibody is described, indicating that the repertoire is not
417 monoclonal. The original antibody isotype, as well as somatic hypermutations, if any, are also
418 shown.
419

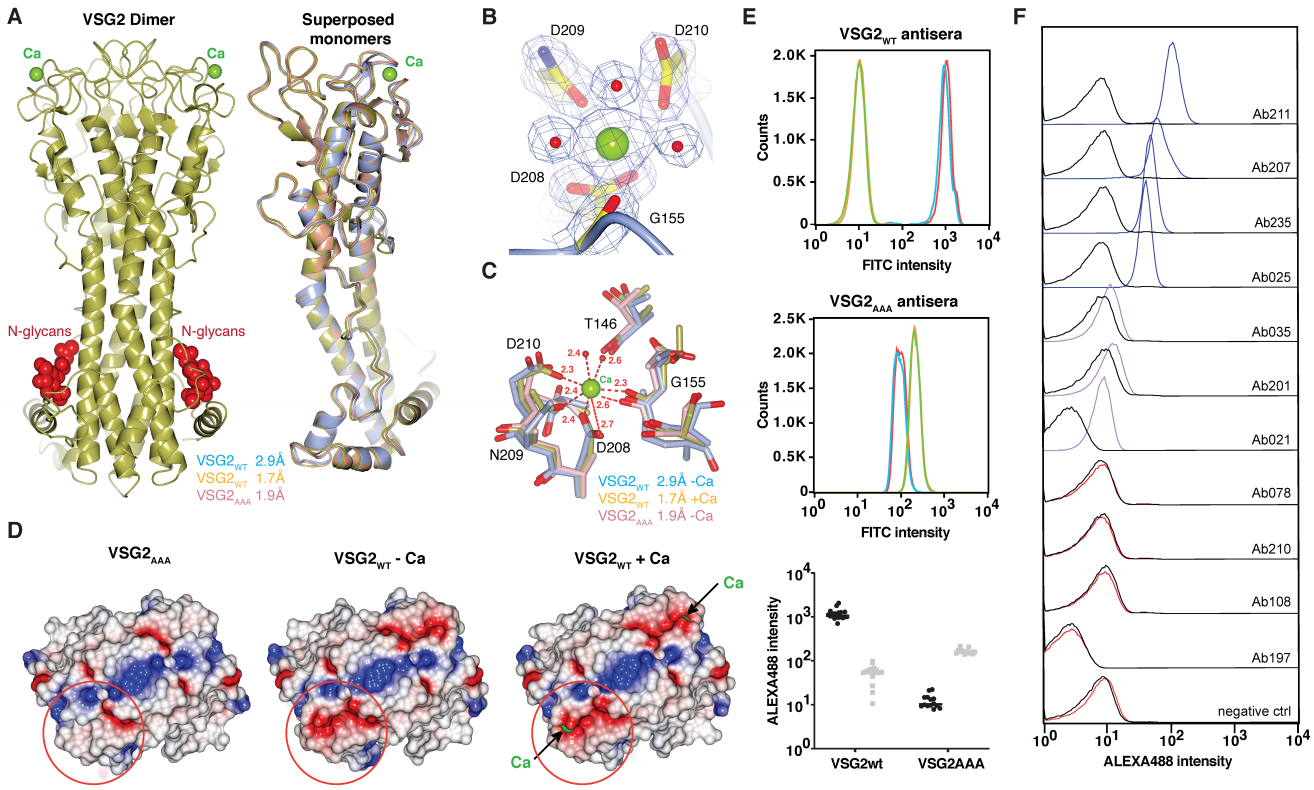

Fig.2: Residues surrounding the calcium binding pocket of VSG2$_{WT}$ define an immunodominant epitope. **(A)** Left - Crystal structure of VSG2$_{WT}$. The homodimer is shown as a ribbon diagram colored in gold, N-linked glycans and calcium atoms are displayed as red and green space-filling atoms, respectively. Right – Structural alignment of monomers of VSG2$_{WT}$ (from left panel, in gold), VSG2$_{WT}$ (from (*16*), in blue) and VSG2$_{AAA}$ (in pink), highlighting the coordination of the calcium atom. **(B)** Close-up of the coordination of calcium binding pocket with corresponding electron density maps. Water molecules and calcium atoms are displayed as red and green space-filling atoms, respectively. **(C)** Superposition of the calcium binding pockets of the 3 structures presented in (A). Water molecules and calcium atoms are displayed as red and green space-filling atoms, respectively. **(D)** Molecular surfaces of VSG2$_{WT}$ + calcium (this study), VSG2$_{WT}$ - calcium (from (*16*)) and VSG2$_{AAA}$. The VSGs are oriented looking 'down' on the top lobe of the protein, the orientation rotated 90° about a horizontal axis in comparison to upper

panels. The surfaces are colored by relative electrostatic potential (blue is basic/positively charged, red is acidic/negatively charged, and white is neutral). **(E)** Histograms reflecting binding intensities of antisera collected from mice infected with $VSG2_{WT}$ and $VSG2_{AAA}$ parasites (top two panels, respectively) with $VSG2_{WT}$ and $VSG2_{AAA}$ parasites (blue and red correspond to 2 independent clones of $VSG2_{WT}$ parasites; green and orange correspond to 2 independent clones of $VSG2_{AAA}$ parasites). Bottom panel shows quantification of binding intensities of antisera collected from mice infected with $VSG2_{WT}$ (black dots) and $VSG2_{AAA}$ (grey dots) parasites with $VSG2_{WT}$ and $VSG2_{AAA}$ parasites (median from n=12-18). **(F)** Histograms reflecting binding intensities of the antibodies presented in Figure 1C with wild type parasites (colors) and AAA-mutant parasites (black). Different colors are meant to distinguish differential binding intensity: red – no binding; purple – poor binding; blue – good binding. The gating strategy is shown in Fig. S12.

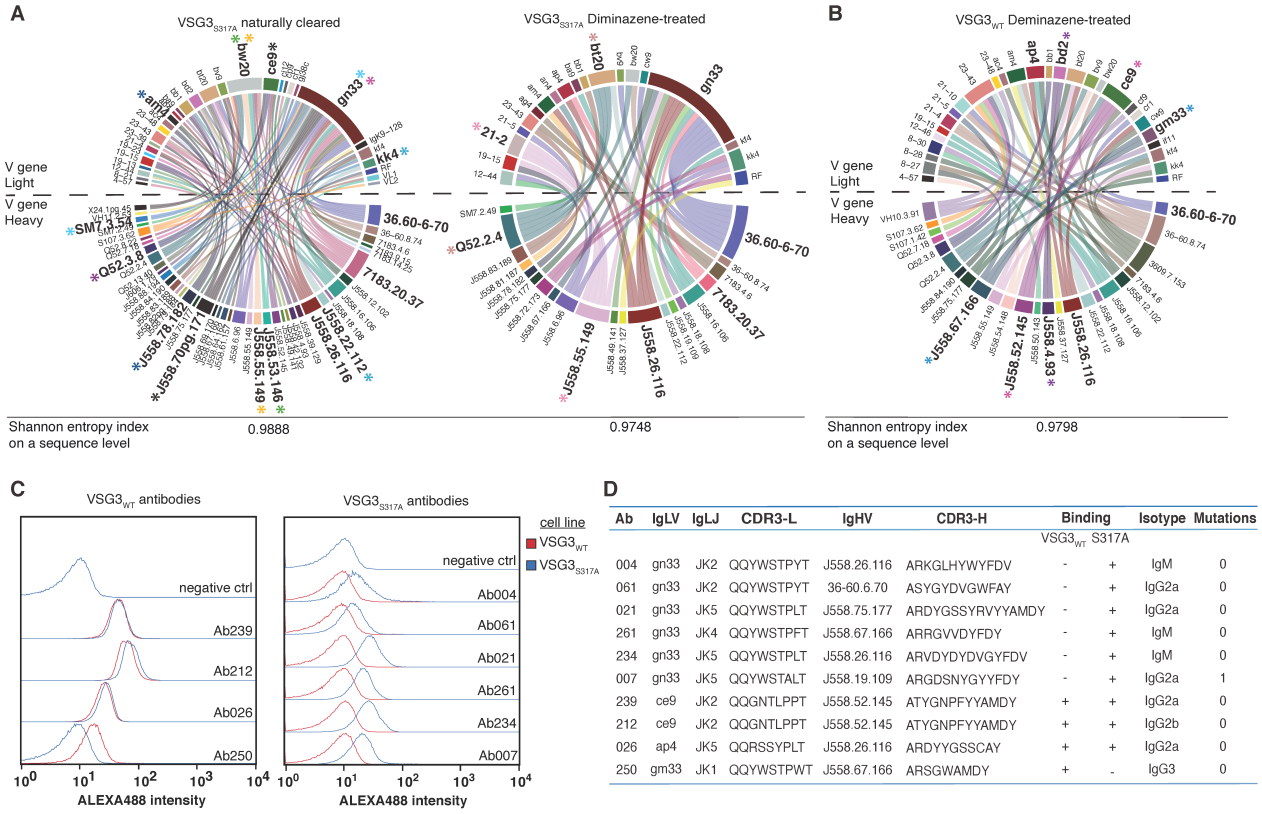

Ab	IgLV	IgLJ	CDR3-L	IgHV	CDR3-H	Binding VSG3WT	Binding S317A	Isotype	Mutations
004	gn33	JK2	QQYWSTPYT	J558.26.116	ARKGLHYWYFDV	-	+	IgM	0
061	gn33	JK2	QQYWSTPYT	36-60.6.70	ASYGYDVGWFAY	-	+	IgG2a	0
021	gn33	JK5	QQYWSTPLT	J558.75.177	ARDYGSSYRVYYAMDY	-	+	IgG2a	0
261	gn33	JK4	QQYWSTPFT	J558.67.166	ARRGVVDYFDY	-	+	IgM	0
234	gn33	JK5	QQYWSTPLT	J558.26.116	ARVDYDYDVGYFDV	-	+	IgM	0
007	gn33	JK5	QQYWSTALT	J558.19.109	ARGDSNYGYYFDY	-	+	IgG2a	1
239	ce9	JK2	QQGNTLPPT	J558.52.145	ATYGNPFYYAMDY	+	+	IgG2a	0
212	ce9	JK2	QQGNTLPPT	J558.52.145	ATYGNPFYYAMDY	+	+	IgG2b	0
026	ap4	JK5	QQRSSYPLT	J558.26.116	ARDYYGSSCAY	+	+	IgG2a	0
250	gm33	JK1	QQYWSTPWT	J558.67.166	ARSGWAMDY	+	-	IgG3	0

Fig.3: VSG3$_{S317A}$ parasites elicit a restricted B cell response, with preferential utilization of a light chain Vκ gene (gn33). (A) Circos diagrams generated for the VSG3$_{S317A}$ V gene signatures of four mice infections, two naturally cleared (left - n=114 pairs) and two diminazene treated (right - n=48 pairs). Different colors depict each heavy chain variable gene (bottom half of the plot), and each light chain variable gene (top half of the plot). The heavy and light chain variable gene pairings that form the antibodies are illustrated as connector lines starting from the heavy chain genes, providing also information about the frequency of the pairings. Genes from both chains that appeared only once and resulted in single heavy-light pairings, were considered background and were removed from the plot. Colored-asterisks depict individual B cells that correspond to clones (ie share the same V heavy and V light gene segments but also the same DJ or J genes and the same CDR3 length and sequence). Shannon entropy shows clonal diversity on a sequence level, a number of 1.0 shows 100% clonal diversity (no clones), while a value of 0.0 corresponds to 0%

456 clonal diversity (only clones). **(B)** Circos plots generated for the $VSG3_{WT}$ V gene signatures from
457 two mice whose infections were treated with diminazene (n=53 pairs), as described in (A). **(C)**
458 Left: FACS analysis of heavy and light chain pairs selected from the $VSG3_{WT}$ repertoire, produced
459 recombinantly as IgG1 antibodies. The plots depict antibody binding to $VSG3_{WT}$ (red) or
460 $VSG3_{S317A}$ (blue) *T. brucei* cells. Parasites were first stained with each antibody supernatant, and
461 counter stained with (mouse anti-human) AlexaFluor488-IgG1 secondary antibody. The gating
462 strategy is shown in Fig. S12. Staining with supernatants from untransfected cells (no plasmid)
463 serves as a negative control. All data are normalized to mode. Right: FACS showing the same
464 experimental setup but now for binding of recombinant antibodies selected from the $VSG3_{S317A}$
465 repertoire. **(D)** Table of all the $VSG3_{S317A}$ antibodies with gn33 as a light chain that bound to the
466 cognate and WT cells, as well as of all the $VSG3_{WT}$ antibodies and their binding to cognate and
467 mutant cells. The (+) symbol indicates binding while the (-) lack of binding. V and J segments as
468 well as the CDR3 of both heavy and light chain genes are shown, along with the binding to the
469 respective parasites. The original antibody isotype, as well as somatic hypermutations, if any, are
470 also shown.
471
472

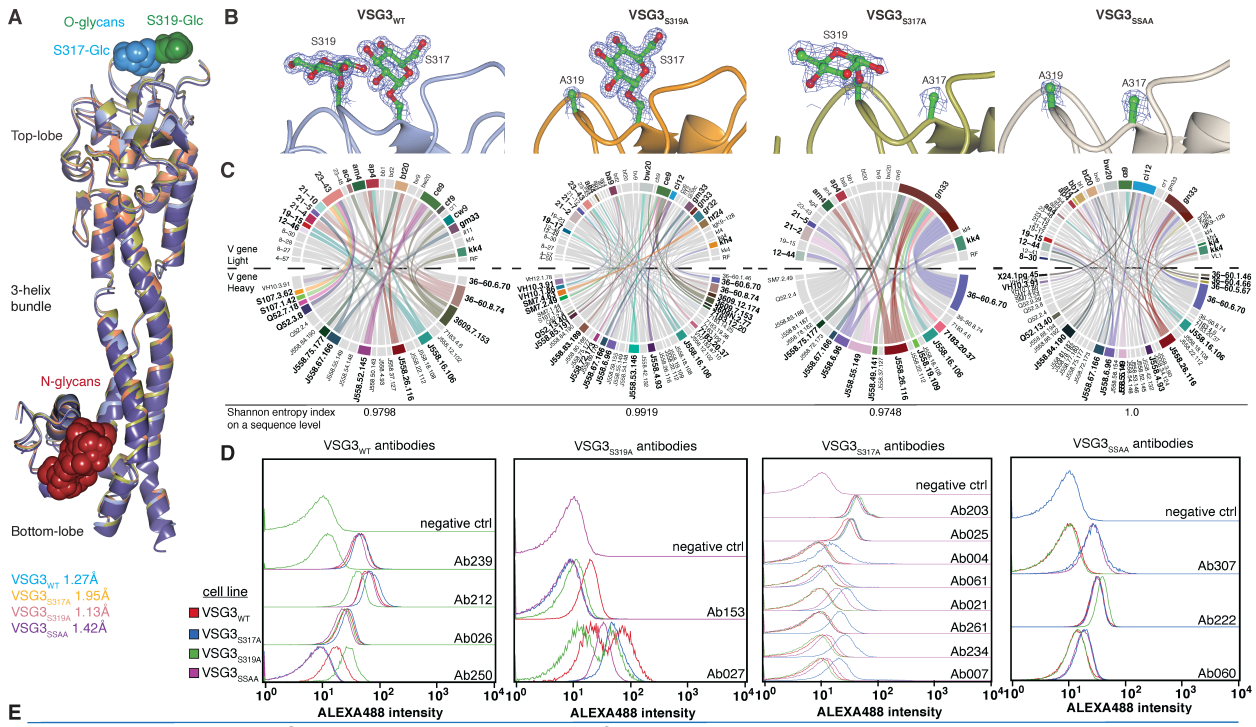

E

Ab	IgLV	IgLJ	CDR3-L	IgHV	CDR3-H	Binding				Isotype	Mutations
						$VSG3_{WT}$	S317A	S319A	SSAA		
234	gn33	JK5	QQYWSTPLT	J558.26.116	ARVDYDYDVGYFDV	-	+	-	-	IgM	0
021	gn33	JK5	QQYWSTPLT	J558.75.177	ARDYGSSYRVYYAMDY	-	+	-	+	IgG2a	0
250	gm33	JK1	QQYWSTPWT	J558.67.166	ARSGWAMDY	+	-	+	-	IgG3	0
222	aa4	JK2	QQYHSYPPT	J558.16.106	ARLFYYGSSPYFDY	+	+	+	+	IgM	0
239	ce9	JK2	QQGNTLPPT	J558.52.145	ATYGNPFYYAMDY	+	+	+	+	IgG2a	0

Fig.4: Nearly identical VSG3 variant coats elicit distinct V gene signatures. **(A)** Overlaid crystal structures of all four VSG3 monomers, shown as ribbon diagrams and colored in blue (WT), gold (S317A), salmon (S319A) and purple (SSAA). The N-glycans are represented as red spheres on the bottom lobe, while the *O*-linked sugars as blue (S317-sugar) and green (S319-sugar) spheres on the top lobe. **(B)** Electron density maps focused on the presence or absence of the S317 and S319 *O*-Glucose molecules for all individual proteins as indicated in the labeling. **(C)** Circos plots of the diminazene-treated plasma cell antibody repertoires (V signatures shown only) of WT (n=53 pairs), S317A (n=48 pairs), S319A (n=109 pairs) and SSAA (n=102 pairs). Different colors depict each heavy chain variable gene (bottom half of the plot), and each light chain variable gene (top half of the plot). The heavy and light chain variable gene pairings that form the antibodies are illustrated as connector lines starting from the heavy chain genes, providing also information about

484 the frequency of the pairings. Genes from both chains that appeared only once and resulted in
485 single heavy-light pairings, were considered background and were removed from the plot. The
486 antibody pairs picked for validation are presented in color, while all other genes are in gray.
487 Shannon entropy shows clonal diversity on a sequence level (a value of 1.0 shows 100% clonal
488 diversity (no clones), while a value of 0.0 corresponds to 0% clonal diversity (only clones)). **(D)**
489 FACS data showing the binding of the validated antibodies, secreted as IgG1s, to $VSG3_{WT}$ (red),
490 $VSG3_{S317A}$ (blue), $VSG3_{S319A}$ (green) and $VSG3_{SSAA}$ (purple) -covered trypanosomes. Parasites
491 were first stained with each antibody supernatant, followed by counter staining with a (mouse anti-
492 human) AlexaFluor488-IgG1 secondary antibody. The gating strategy is shown in Fig. S12.
493 Staining with supernatants from untransfected cells (no plasmid) is used as a negative control. All
494 data were normalized to mode. **(E)** Table of representative binding patterns of the produced
495 antibodies (also in 4D) to different trypanosome cell lines. The (+) symbol indicates binding while
496 the (-) non-binding. V and J segments as well as the CDR3 of both heavy and light are shown,
497 along with the binding to the individual cell lines. The original isotypes and somatic
498 hypermutations, if any, are also listed.

499